Aldehyde dehydrogenase 3A1 activation prevents radiation-induced xerostomia by protecting salivary stem cells from toxic aldehydes

Julie P. Saiki[a], Hongbin Cao[b], Lauren D. Van Wassenhove[a], Vignesh Viswanathan[b], Joshua Bloomstein[b], Dhanya K. Nambiar[b], Aaron J. Mattingly[c], Dadi Jiang[b], Che-Hong Chen[a], Matthew C. Stevens[a], Amanda L. Simmons[b], Hyun Shin Park[d], Rie von Eyben[b], Eric T. Kool[d], Davud Sirjani[e], Sarah M. Knox[c], Quynh Thu Le[b,1], and Daria Mochly-Rosen[a,1]

[a]Department of Chemical and Systems Biology, Stanford University School of Medicine, Stanford, CA 94305; [b]Department of Radiation Oncology, Stanford University School of Medicine, Stanford, CA 94305; [c]Department of Cell and Tissue Biology, University of California San Francisco, CA 94143; [d]Department of Chemistry, Stanford University, Stanford, CA 94305; and [e]Department of Otolaryngology–Head and Neck Surgery, Stanford University School of Medicine, Stanford, CA 94305

Edited by Anton Berns, The Netherlands Cancer Institute, Amsterdam, The Netherlands, and approved May 4, 2018 (received for review February 8, 2018)

Xerostomia (dry mouth) is the most common side effect of radiation therapy in patients with head and neck cancer and causes difficulty speaking and swallowing. Since aldehyde dehydrogenase 3A1 (ALDH3A1) is highly expressed in mouse salivary stem/progenitor cells (SSPCs), we sought to determine the role of ALDH3A1 in SSPCs using genetic loss-of-function and pharmacologic gain-of-function studies. Using DarkZone dye to measure intracellular aldehydes, we observed higher aldehyde accumulation in irradiated *Aldh3a1*$^{-/-}$ adult murine salisphere cells and in situ in whole murine embryonic salivary glands enriched in SSPCs compared with wild-type glands. To identify a safe ALDH3A1 activator for potential clinical testing, we screened a traditional Chinese medicine library and isolated D-limonene, commonly used as a food-flavoring agent, as a single constituent activator. ALDH3A1 activation by D-limonene significantly reduced aldehyde accumulation in SSPCs and whole embryonic glands, increased sphere-forming ability, decreased apoptosis, and improved submandibular gland structure and function in vivo after radiation. A phase 0 study in patients with salivary gland tumors showed effective delivery of D-limonene into human salivary glands following daily oral dosing. Given its safety and bioavailability, D-limonene may be a good clinical candidate for mitigating xerostomia in patients with head and neck cancer receiving radiation therapy.

ALDH3A1 | aldehyde dehydrogenase | radiation | dry mouth | xerostomia

Xerostomia, the experience of dry mouth due to hyposalivation, is the most common side effect of radiation therapy for head and neck cancer (HNC) (1, 2). Acute or chronic hyposalivation can impair speaking and swallowing and increases the risk of oral pain, ulcerations, infections, and dental caries. Submandibular glands (SMGs) contribute more than 60% of unstimulated saliva and are essential for resting salivation and oral lubrication (2). Despite advances in intensity-modulated radiation therapy for HNC, ∼40% of patients develop xerostomia (3, 4). Current treatments are suboptimal, limited to temporary symptom relief and amifostine, a reactive oxygen species (ROS) scavenger administered by i.v. infusion with limited efficacy and poor tolerability (1, 2, 5–11).

Salivary functional recovery after ionizing irradiation (IR) likely depends on the number of surviving salivary stem/progenitor cells (SSPCs) in the gland (12). If SSPCs survive the IR, they can self-renew and regenerate the damaged salivary gland tissue. This regenerative capacity is evident from transplantation studies of rodent and human SSPCs into irradiated rodent salivary glands, which resulted in improved saliva production (13–18) and tissue homeostasis (19). However, adult SSPCs make up less than 0.5% of the total cell population, and their limited numbers pose a challenge for their use in stem cell therapy (14, 20–24). After IR, ROS react with cellular components to generate aldehydes that readily diffuse between cells and form adducts on proteins, nucleic acids, and lipids, thus damaging cells (25–27). Our research therefore focused on reducing IR-induced toxic aldehydes in irradiated SMGs to protect the critical SSPC population. These aldehydes are cleared by aldehyde dehydrogenases (ALDHs), which protect cells from injury. Of the 19 cytoprotective ALDH family members found in humans (25), ALDH3A1 and ALDH1A1 are most abundant in stem cells (28). We previously reported that ALDH3A1 RNA is highly expressed in an SSPC-enriched population (Lin$^-$CD24$^+$c-Kit$^+$sca-1$^+$) (17) and that a small-molecule activator of ALDH3A1 (Alda-89) that we identified (29) increases SSPC-enriched cells (c-Kit$^+$/CD90$^+$) and their sphere-forming ability (20). We also found that Alda-89 treatment increases mouse saliva production and preserves acini after IR (30). However, the role of ALDH3A1 in SSPCs is unknown, and Alda-89 (safrole) has carcinogenic properties and cannot be used in patients (31). Here, we investigated the role of ALDH3A1 in scavenging toxic aldehydes in SSPCs using genetic loss-of-function and pharmacologic gain-of-function studies. We also identified a safe ALDH3A1 activator that prevents hyposalivation after radiation by decreasing aldehyde

Significance

Radiation therapy for head and neck cancer often leads to dry mouth, a debilitating condition that affects speaking, swallowing, and other functions related to quality of life. Since salivary functional recovery after radiation is largely dependent on the number of surviving salivary stem/progenitor cells (SSPCs), we reasoned that protection of SSPCs from injury is critical for mitigating dry mouth. Following radiation, SSPCs accumulate toxic aldehydes that damage DNA, proteins, and lipids, leading to cell death. Here, we identified D-limonene as an activator of aldehyde dehydrogenase 3A1 (ALDH3A1) with a favorable safety profile for clinical use. ALDH3A1 activation decreases aldehyde accumulation in SSPCs, increases sphere-forming ability, reduces apoptosis, and preserves salivary gland structure and function following radiation without reducing the anticancer effects.

Author contributions: J.P.S., C.-H.C., E.T.K., S.M.K., Q.T.L., and D.M.-R. designed research; J.P.S., H.C., L.D.V.W., V.V., J.B., D.K.N., A.J.M., D.J., M.C.S., A.L.S., D.S., and S.M.K. performed research; H.S.P. contributed new reagents/analytic tools; J.P.S. and R.v.E. analyzed data; and J.P.S., Q.T.L., and D.M.-R. wrote the paper.

The authors declare no conflict of interest.

This article is a PNAS Direct Submission.

This open access article is distributed under Creative Commons Attribution-NonCommercial-NoDerivatives License 4.0 (CC BY-NC-ND).

[1]To whom correspondence may be addressed. Email: qle@stanford.edu or mochly@stanford.edu.

This article contains supporting information online at www.pnas.org/lookup/suppl/doi:10.1073/pnas.1802184115/-/DCSupplemental.

Published online May 24, 2018.

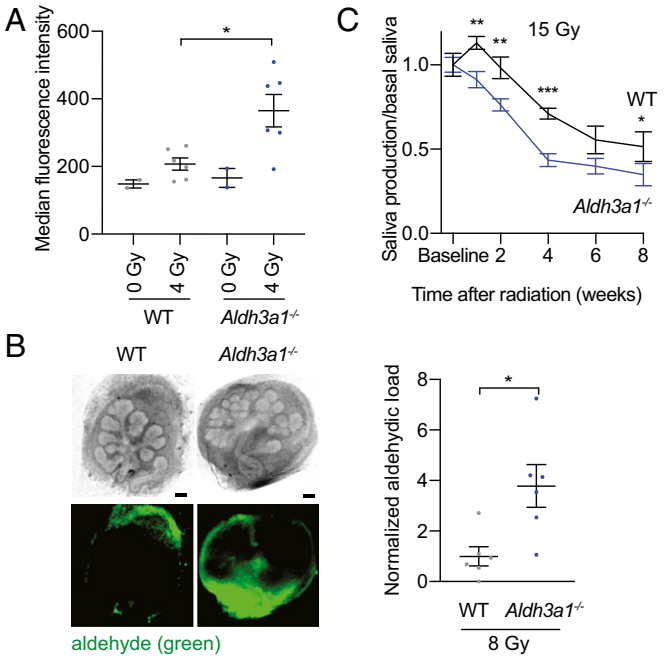

Fig. 1. Loss of ALDH3A1 increases aldehyde accumulation in SSPCs and accelerates hyposalivation after radiation. (*A*) Aldehyde levels in dissociated WT and *Aldh3a1*$^{-/-}$ murine salispheres 2 h after IR, measured as median fluorescence intensity of DarkZone dye by FACS (n = 2–6; bars indicate SEM; *P < 0.05). The experiment was repeated in *SI Appendix*, Fig. S1*A*. (*B*, *Left*) Representative images of WT (*Left*) and *Aldh3a1*$^{-/-}$ (*Right*) E13.5 mouse SMGs after 24 h in culture, treated with DarkZone dye, 3 h after IR, in brightfield (*Upper Row*) and with a florescence filter (*Lower Row*). (Scale bars: 50 μm.) (*Right*) Quantification of DarkZone dye fluorescence intensity of embryonic SMGs, normalized to WT (n = 6; bars indicate SEM; *P < 0.05). (*C*) Pilocarpine-induced saliva production collected in female C57BL/6J WT and *Aldh3a1*$^{-/-}$ mice at baseline and 1, 2, 4, 6, and 8 wk after 15-Gy IR (single dose) (n = 8–11; bars indicate SEM; *P < 0.05; **P < 0.01; ***P < 0.001).

levels and increasing SSPC survival without reducing the anticancer benefit of radiation treatment.

Results

Loss of ALDH3A1 Leads to Increased Aldehyde Levels in SSPCs After Radiation and Accelerates Hyposalivation. To determine the role of ALDH3A1 in aldehyde clearance after IR in SSPCs, we first investigated whether IR increases aldehyde formation in both adult and embryonic murine SSPCs and whether ALDH3A1 is required for aldehyde removal. Dissociated salivary spheres (salispheres) enriched in SSPCs were cultured from adult WT and *Aldh3a1*$^{-/-}$ murine SMGs, irradiated, and treated with a DarkZone dye that fluorescently labels intracellular aldehydes (32). IR (4 Gy) of salispheres increased the fluorescence intensity of WT by ∼30% (Fig. 1*A* and *SI Appendix*, Fig. S1). Moreover, irradiated *Aldh3a1*$^{-/-}$ salispheres displayed ∼75% greater fluorescence intensity than WT, demonstrating that ALDH3A1 is necessary for intracellular aldehyde removal after IR (Fig. 1*A*). Using DarkZone, we also measured aldehyde levels in situ in ex vivo SMGs removed from E13.5 WT and *Aldh3a1*$^{-/-}$ embryos enriched in SSPCs (33). *Aldh3a1*$^{-/-}$ embryonic SMGs had approximately fourfold higher fluorescence intensity than WT SMGs after IR, further demonstrating that ALDH3A1 plays a critical role in removing aldehydes in SSPCs (Fig. 1*B*). DarkZone was most apparent in the mesenchyme, likely due to the ability of aldehydes to diffuse rapidly through membranes and their trapping by DarkZone in the dense fibroblastic mesenchyme.

To determine whether ALDH3A1's ability to scavenge aldehydes in SSPCs affects salivary function after IR, we compared saliva production in WT and *Aldh3a1*$^{-/-}$ mice before and after 15-Gy IR (Fig. 1*C* and *SI Appendix*, Fig. S2). *Aldh3a1*$^{-/-}$ mice exhibited decreased saliva production after IR compared with WT mice, suggesting that ALDH3A1 is required, in part, to protect SMG function after IR.

Identification of D-Limonene, an Activator of ALDH3A1. To determine if ALDH3A1 activation is sufficient to protect salivary glands from IR, we screened for a safe and specific ALDH3A1 activator using a library of 135 traditional Chinese medicine (TCM) extracts (Sun Ten Pharmaceutical Co.). Because TCM extracts have a long history of human use, we reasoned that identified activators would have a higher likelihood of being safe for clinical use. Seven extracts increased ALDH3A1 activity (see list in *SI Appendix*, Fig. S3). HPLC fractionation of these extracts and NMR characterization of the fractions identified several single-molecule constituents that activate ALDH3A1 in a dose-dependent manner (Fig. 2*A*). All identified active constituents were monoterpenes, which are commonly found in plant essential oils and may explain the high hit rate observed in TCM plant extracts. Of these, we identified D-limonene as the active component present in three extracts (*Citrus reticulata*, *Nelumbo nucifera*, and *Anemarrhena asphodeloides*) with the lowest EC_{50} (∼14 μM) and a maximal activity of ∼4.6 (Fig. 2*A*). D-limonene occurs naturally in citrus fruit oils and bears the Food and Drug Administration designation of "generally recognized as safe" (as a food-flavoring agent) under the *Code of Federal Regulations Title 21*. D-limonene has an estimated maximum tolerated dose of 8 g·m^{-2}·d^{-1} (∼15 g/d) (34) and no known risk of mutagenicity, carcinogenicity, or nephrotoxicity in humans (35). Given its potency and favorable safety profile, it is a good candidate for clinical investigation.

To characterize D-limonene's enzymatic activity, we observed that both D-limonene and Alda-89 increase the catalytic activity of ALDH3A1 toward small aldehydes, such as acetaldehyde and propionaldehyde, but not toward aromatic or long-chain aldehydes (Fig. 2*B*). Furthermore, D-limonene appears ALDH3A1-specific and does not increase the activity of the highly homologous ALDH family members ALDH1A1, ALDH2, ALDH3A2, ALDH4A1, ALDH5A1, or ALDH7A1 (Fig. 2*C*). To confirm the specificity of D-limonene for ALDH3A1, we measured the effect of D-limonene on ALDH activity in WT and *Aldh3a1*$^{-/-}$ salisphere lysates and observed that D-limonene increases the ALDH activity of WT lysate by ∼30% but not that of *Aldh3a1*$^{-/-}$ lysate, which exhibited lower basal activity (Fig. 2*D*). D-limonene may increase the catalytic activity of ALDH3A1 by reducing the size of the catalytic tunnel, thus increasing the number of productive interactions between the substrate and the catalytic Glu_{333} while simultaneously protecting Cys_{243} from adduction and inactivation by the substrate (Fig. 2*E*, *Left*). This effect is similar to observations for ALDH2 and Alda-1, an activator of ALDH2 (36). The selectivity of D-limonene for ALDH3A1, relative to ALDH2, may be due to the size of the catalytic tunnel of these enzymes. D-limonene fits in the catalytic tunnel of ALDH3A1 without blocking the catalytically critical Glu_{333} (Fig. 2*E*, *Lower Left*), whereas in ALDH2, access to this catalytic glutamate (Glu_{268} in ALDH2) appears hindered (Fig. 2*E*, *Lower Right*).

ALDH3A1 Activation with D-Limonene Reduces Aldehydic Load, Improves Sphere Growth, and Mitigates Hyposalivation in Vivo After Radiation. Based on the above observations, we hypothesized that ALDH3A1 activation with D-limonene would reduce IR-induced aldehyde levels in SSPCs. Using DarkZone, we observed that D-limonene treatment of irradiated WT salispheres decreased the aldehydic load to nearly nonirradiated levels compared with vehicle control (Fig. 3*A*). In contrast, post-IR aldehyde levels in D-limonene–treated and nontreated *Aldh3a1*$^{-/-}$ salispheres were not statistically different (*SI Appendix*, Fig. S4). Furthermore, D-limonene treatment of irradiated ex vivo E13.5 SMGs also reduced

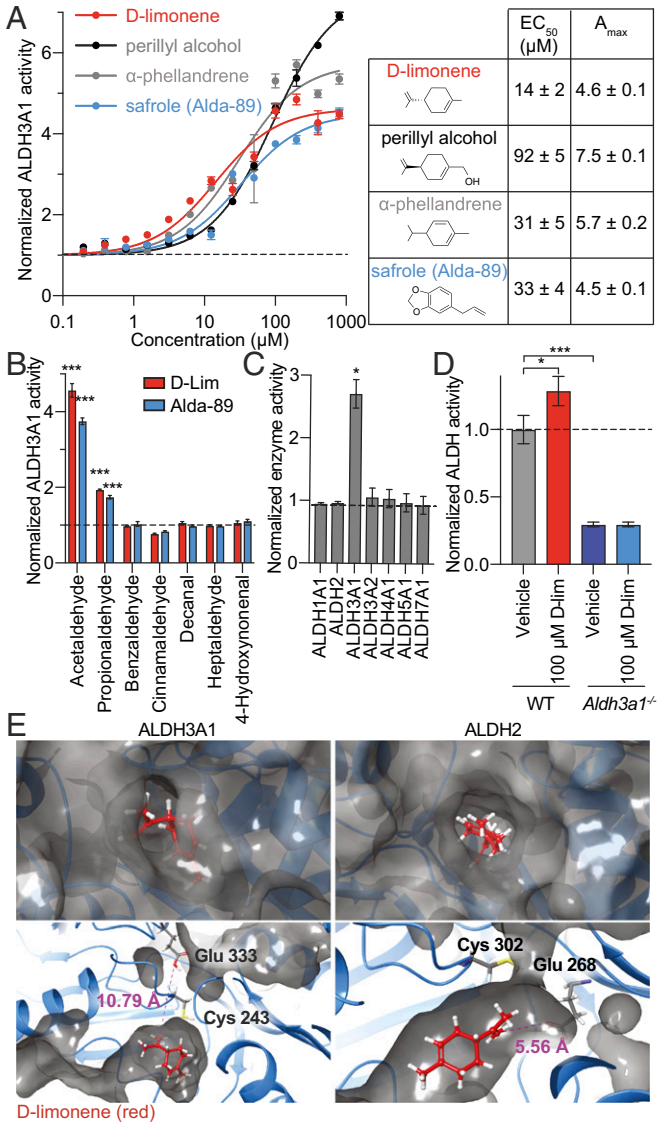

Fig. 2. The natural product library screen identifies D-limonene as a small-molecule activator of ALDH3A1. (*A*) ALDH3A1 activator dose–response curves for three top single active ingredients identified from a TCM library screen (6 nM to 400 μM) and Alda-89 (29), measured by spectrophotometric enzyme activity assay and normalized to baseline activity ($n = 3$; bars indicate propagated error). (*B*) Effect of 100 μM D-limonene or Alda-89 on ALDH3A1 enzyme activity using 10 mM indicated aldehyde or 200 μM aliphatic 4-hydroxynonenal ($n = 3$; bars indicate propagated error; ***$P < 0.001$). (*C*) Enzyme activities of ALDH isozymes using 5 μg/mL of recombinant enzyme, 10 mM acetaldehyde as the substrate, and 20 μM D-limonene ($n = 3$; bars indicate propagated error; *$P < 0.05$). (*D*) Enzyme activity of 400 μg/mL of murine WT and *Aldh3a1*$^{-/-}$ salisphere lysate with 10 mM acetaldehyde by fluorescence-coupled enzymatic activity assay ($n = 3$; bars indicate propagated error; *$P < 0.05$, ***$P < 0.001$). (*E*, *Upper Left*) Surface view of D-limonene (red) docked to ALDH3A1. (*Lower Left*) Interior view of ALDH3A1 showing D-limonene (red) docked within the catalytic tunnel 10.79 Å from the catalytic glutamate Glu333 at the closest approach. Note: The surface is not shown as continuous, but the catalytic tunnel extends past the catalytic cysteine Cys243. (*Upper Right*) Surface view of D-limonene (red) docked to ALDH2. (*Lower Right*) Interior view of ALDH2 showing D-limonene (red) docked within the catalytic tunnel 5.56 Å from the catalytic glutamate Glu268 at the closest approach.

aldehyde levels by approximately fourfold compared with vehicle control, to nearly basal levels (Fig. 3*B*). These data indicate that D-limonene treatment reduces aldehydes after IR in both adult and embryonic SSPCs.

To determine whether D-limonene protects SSPCs after radiation, we measured the ability of dissociated SMG cells to form salispheres after IR. Compared with cells from mice that received no treatment, dissociated SMG cells from D-limonene–treated mice 24 h after 15-Gy IR demonstrated an approximately twofold increase in sphere-forming ability (Fig. 3*C*), and cells from D-limonene–treated mice 20 wk after 30-Gy IR demonstrated an approximately 30-fold increase in sphere-forming ability (Fig. 3*D*). These data suggest that D-limonene improves both short- and long-term SSPC survival after IR.

We next determined whether D-limonene can protect salivary gland structure and function after IR in vivo in mice. After collection of baseline saliva, the treatment group received D-limonene daily in chow starting 1 wk before IR. Measurement of D-limonene levels by GC-MS showed that oral D-limonene treatment for 2 wk led to drug levels in murine SMGs of ∼7,000 ng/g (mean $7.0 \pm 1.0 \times 10^3$ ng/g, SEM; $n = 5$). Mice were irradiated with 15 Gy, and, in a second experiment, with 30 Gy (6 Gy/d). In both experiments, D-limonene–treated mice had significantly more saliva production after IR than nontreated mice (Fig. 3*E* and *SI Appendix*, Fig. S5 *A* and *B*). Eight weeks after 30-Gy IR, Periodic acid Schiff (PAS) staining for acinar cells showed that D-limonene–treated SMGs maintained ∼90% preservation of the acinar area (relative to nonirradiated glands) compared with <30% for the irradiated control group (*SI Appendix*, Fig. S5*C*). In a third experiment, we irradiated mice with 30 Gy, began daily D-limonene starting 24 h after the final IR dose, and collected saliva up to 20 wk after IR. The treatment group again sustained significantly higher saliva levels than the nontreated group (Fig. 3*F* and *SI Appendix*, Fig. S5*D*). Consistent with these data, PAS staining of SMGs 20 wk after 30-Gy IR showed greater than three times more acinar cell preservation with D-limonene treatment compared with the nontreated group (Fig. 3*G*). D-limonene did not increase saliva production in nonirradiated mice (*SI Appendix*, Fig. S5*E*).

To learn whether D-limonene affects tumor growth or reduces the radiation effect on cancer, we implanted SCID mice with either SAS [human papillomavirus (HPV)-negative] or SCC90 (HPV-positive) HNC squamous cell carcinoma cells s.c. and treated them with or without D-limonene and with or without IR to the tumor site. D-limonene treatment did not promote tumor growth (*SI Appendix*, Fig. S6 *A* and *C*) or lessen the antitumor effects of IR (*SI Appendix*, Fig. S6 *B* and *D*).

ALDH3A1 Activation Reduces Apoptosis in SMGs. To determine how ALDH3A1 activation and reduced aldehyde levels protect salivary gland structure and function after IR, we performed RNA-sequencing (RNA-seq) studies on EpCAM$^+$ cells enriched in SSPCs (33) isolated from WT and *Aldh3a1*$^{-/-}$ murine SMGs 2 wk after 30-Gy IR. These data showed an increase in apoptotic-related gene expression after IR, which was exacerbated in *Aldh3a1*$^{-/-}$ cells (Fig. 4*A*, *Left*) but suppressed with D-limonene treatment (Fig. 4*A*, *Right*). To determine the role of ALDH3A1 on early and late apoptosis in SSPCs, we stained dissociated murine EpCAM$^+$ cells isolated from WT and *Aldh3a1*$^{-/-}$ SMGs with annexin V (an apoptosis marker) and propidium iodide (PI) and observed that *Aldh3a1*$^{-/-}$ cells had approximately 2.2-fold more early and late apoptotic cells than the vehicle-treated control (Fig. 4*B*). We then tested the effect of D-limonene on apoptosis in irradiated WT EpCAM$^+$ cells and observed ∼60% fewer early and late apoptotic cells compared with the irradiated vehicle-treated control (Fig. 4*C*). Furthermore, we stained murine SMGs removed immediately after 30-Gy IR (6 Gy/5 d) with cleaved caspase-3, a marker of apoptosis activation. Irradiated SMGs had a greater than fivefold increase in apoptotic cells compared with nonirradiated SMGs, and D-limonene treatment in chow reduced apoptosis to nearly nonirradiated levels (Fig. 4*D*). RNA-seq of irradiated EpCAM$^+$ cells isolated from WT mice 2 wk after 30-Gy IR to the SMG also showed a correlation between D-limonene treatment and increased

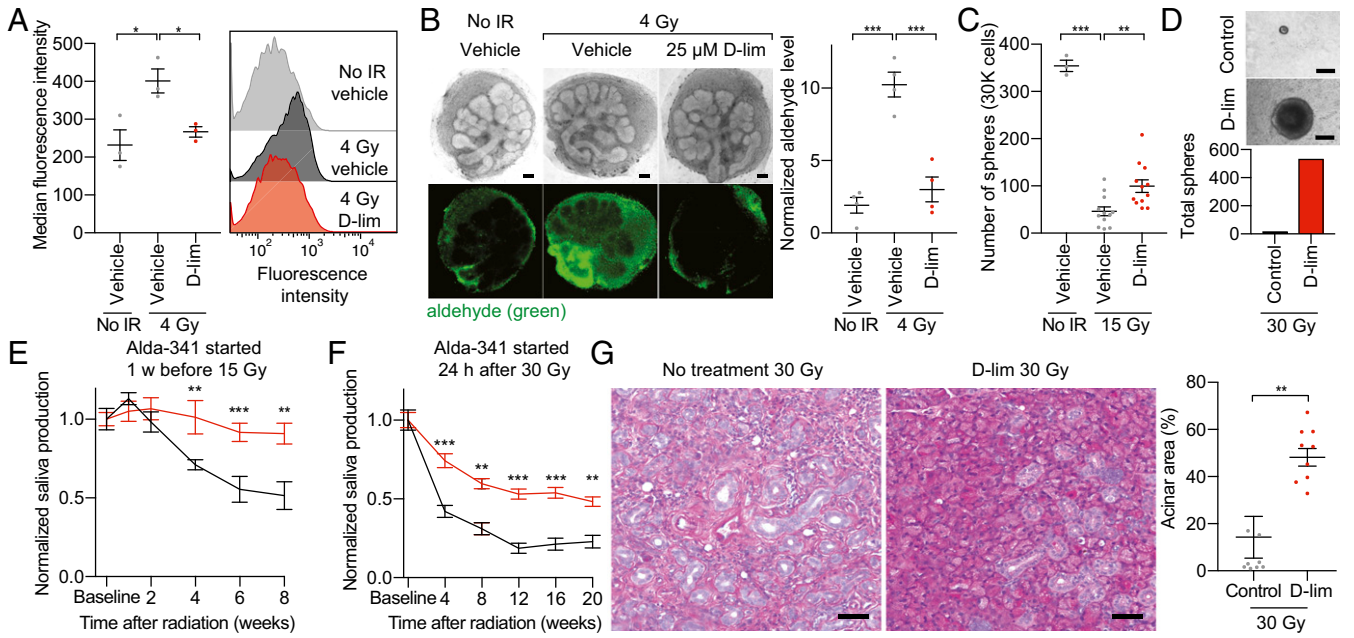

Fig. 3. D-limonene reduces aldehyde levels after IR and mitigates IR-induced hyposalivation in vivo. (*A*, *Left*) Aldehyde levels in dissociated salispheres 2 h after IR treated with 100 μM D-limonene or vehicle (PEG-400) control, measured as median fluorescence intensity of DarkZone dye. (*Right*) Representative histograms of the fluorescence intensity of 10,000 cells ($n = 3$; bars indicate SEM; $^*P < 0.05$). (*B*, *Left*) Representative images of E13.5 SMGs cultured for 24 h with 25 μM D-limonene or vehicle (PEG-400) control, incubated with DarkZone dye, and imaged 3 h after IR with brightfield (*Upper Row*) and a fluorescence filter (*Lower Row*). (Scale bars: 100 μm.) (*Right*) Quantified aldehyde levels measured as average fluorescence intensity per gland area and normalized to nonirradiated vehicle control ($n = 4$; bars indicate SEM; $^{***}P < 0.001$). (*C*) Number of spheres grown from 30,000 dissociated SMG cells from mice 24 h after a single dose of 15 Gy. The treatment group received daily D-limonene in chow starting 7 d before IR. (no IR control: $n = 3$; IR groups: $n = 12$; bars indicate SEM; $^{**}P < 0.01$; $^{***}P < 0.001$.) (*D*, *Upper*) Representative images of spheres grown from dissociated SMG cells from mice 20 wk after 30-Gy IR (6 Gy/d). The treatment group received daily D-limonene starting 24 h after IR. (Scale bars: 50 μm.) (*Lower*) Total number of spheres counted from each group ($n = 4$ SMGs per group). (*E*) Saliva was measured in female C57BL/6J mice at baseline and 1, 2, 4, 6, and 8 wk after a single dose of 15 Gy. The treatment group started daily 10% D-limonene 7 d before IR ($n = 7$–8; bars indicate SEM; $^{**}P < 0.01$; $^{***}P < 0.001$). (*F*) Saliva was measured in female C57BL/6J mice at baseline and every 4 wk after 30-Gy IR (6 Gy/d). The treatment group started daily 10% D-limonene 24 h after the final IR fraction. ($n = 7$–8; bars indicate SEM; $^{**}P < 0.01$; $^{***}P < 0.001$). (*G*, *Left*) Representative images of mouse SMGs 20 wk after IR, stained with PAS. (Scale bars: 50 μm.) (*Right*) Quantification of the SMG acinar area 20 wk after IR using 10 random images per group ($n = 6$–14 SMGs; bars indicate SEM, $^{**}P < 0.01$).

expression of genes related to glutathione metabolism, which reduces oxidative stress, and decreased expression of immune response-related genes (*SI Appendix*, Fig. S7 *A* and *B*).

Distribution of Oral D-Limonene to Human Salivary Glands. To assess the feasibility of D-limonene as an oral therapy for radiation-induced xerostomia, we initiated a phase 0 study to determine whether oral D-limonene is distributed to human salivary glands. Patients scheduled to undergo surgical removal of a salivary gland tumor were given 2 g/d oral D-limonene (1 g twice daily) for 2 wk immediately before their scheduled surgery. Saliva and plasma were collected at baseline and on the day of surgery, and normal salivary tissue was collected at surgery. D-limonene was measured in plasma, saliva, and gland tissue by GC-MS. Data from four patients showed that D-limonene was present at high levels in the salivary gland, measuring on average ~2,000 ng/g (Fig. 5*A* and *SI Appendix*, Table S1*A*). This is within the same order of magnitude as drug levels measured in murine salivary glands after 2 wk of 10% D-limonene delivered in chow (~7,000 ng/g), suggesting that this dose may be sufficient to achieve a clinical benefit. D-limonene levels were lower in saliva and blood, possibly due to the compound's hydrophobic properties (Fig. 5 *B* and *C* and *SI Appendix*, Table S1 *B* and *C*).

Discussion

Adult SSPCs are thought to enable the repair of damaged salivary glands and thereby mitigate xerostomia after radiation therapy in patients with HNC (37). Using a combination of loss- and gain-of-function studies, we demonstrated that IR increases aldehyde production in SSPCs, which likely contributes to their injury and death after IR. Furthermore, we showed that ALDH3A1 increases aldehyde clearance in both adult salisphere cells and embryonic SMGs. ALDH3A1 activation with D-limonene further enhanced aldehyde metabolism in SSPCs beyond normal basal function, reduced apoptosis, and increased survival after IR, as evinced by increased sphere-forming ability after IR in treated mice. Importantly, D-limonene reduced hyposalivation and improved acinar survival in vivo after IR. Although we cannot rule out the possibility that the effect of D-limonene in vivo could be mediated by additional pathways or could originate from other cell types, the combined data presented here show that ALDH3A1 plays an important role in protecting SSPCs from IR-induced injury by increasing aldehyde scavenging.

D-limonene is a major component in citrus peel oil and is a common food flavoring. Clinical studies evaluating D-limonene's activity in patients with refractory solid tumors (34) or those with early breast cancer undergoing surgery (38) suggest that D-limonene has an acceptable safety profile for cancer patients at clinically relevant doses. Our preclinical studies indicated that ALDH3A1 activation with D-limonene did not promote tumor growth or protect tumors from radiation in vivo. Similarly, higher ALDH3A1 protein levels in human HNC tumors were not associated with worse prognosis (30). We therefore proceeded with a phase 0 human study and observed that D-limonene concentrates at high levels in human salivary glands. Further investigation is needed to determine whether these levels are sufficient to protect human SSPCs from radiation damage.

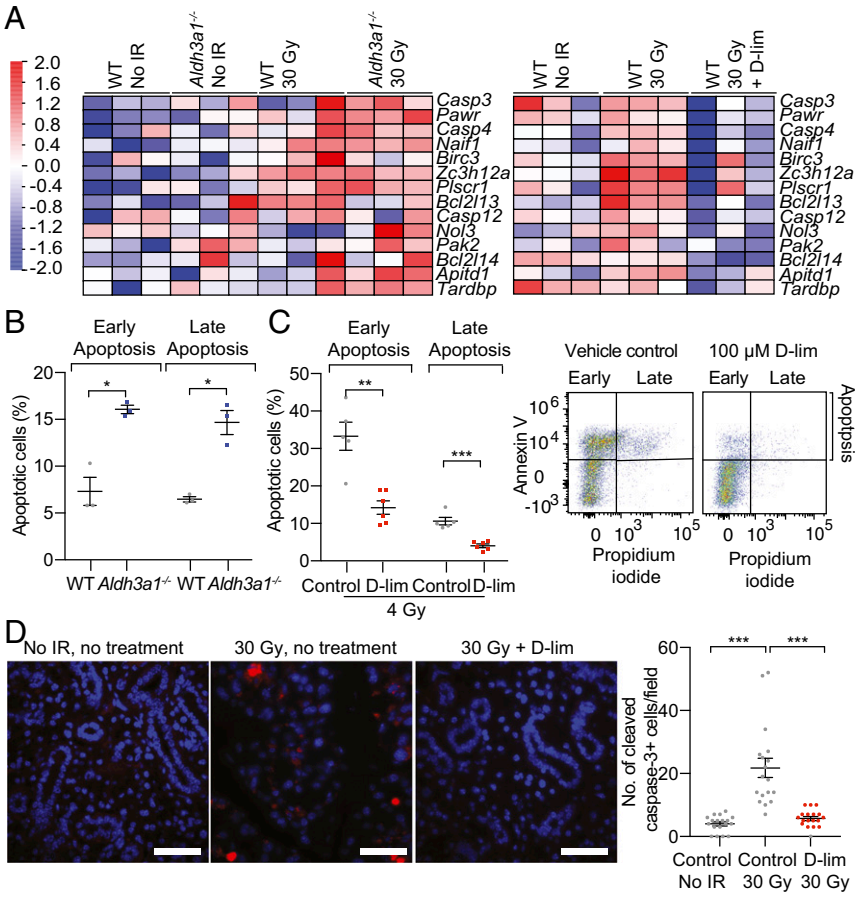

Fig. 4. D-limonene reduces apoptosis. (*A*, *Left*) Heatmap of the apoptotic RNA signature of WT and *Aldh3a1*$^{-/-}$ EpCAM$^+$ cells from murine SMGs 2 wk after 30-Gy IR (6 Gy/d). (*Right*) Heatmap of the apoptotic RNA signature of WT SMG EpCAM$^+$ cells 2 wk after 30-Gy IR (6 Gy/d) isolated from mice treated or not treated with daily 10% D-limonene starting 7 d before IR. (*B*) Percentage of early (annexin V$^+$PI$^-$) and late (annexin V$^+$PI$^+$) apoptotic nonirradiated EpCAM$^+$ WT and *Aldh3a1*$^{-/-}$ SMG cells by FACS analysis ($n = 3$; bars indicate SEM; $^*P < 0.05$). (*C*, *Left*) Percentage of early and late apoptotic WT EpCAM$^+$ SMG cells treated with 100 μM D-limonene or vehicle (PEG-400) control 18 h after 4-Gy IR by FACS analysis ($n = 5$–6; bars indicate SEM; $^{**}P < 0.01$; $^{***}P < 0.001$). (*Center*) FACS dot-plot for control vehicle-treated cells. (*Right*) FACS dot-plot for D-limonene–treated cells. (*D*, *Left*) Representative images of cleaved caspase-3 (red) and DAPI (blue) staining of fixed SMGs removed immediately after the final fraction of 30-Gy IR (6 Gy/d). The treatment group began 10% D-limonene 7 d before IR. (Scale bars: 50 μm.) (*Right*) The number of cleaved caspase-3$^+$ cells (red) per field blindly counted ($n = 6$–7 SMGs, 18 images; bars indicate SEM; $^{***}P < 0.001$).

Materials and Methods

See *SI Appendix, Supplemental Methods* for experimental details.

Animals. C57BL/6J and SCID mice were purchased from Jackson Laboratories, and C57BL/6J *Aldh3a1*$^{-/-}$ mice were obtained from the laboratory of Vasilis Vasiliou at Yale School of Public Health, New Haven, CT (39). Timed pregnant CD-1/ICR mice were purchased from Envigo. The Administrative Panel on Laboratory Animal Care at Stanford University and the Institutional Animal Care and Use Committee at the University of California, San Francisco approved all animal protocols.

DarkZone Dye Aldehyde Assay in Murine Salispheres and ex Vivo E13.5 Whole SMGs. Primary salivary gland cells were grown into spheres as previously described (40). Dissociated spheres were incubated with 20 μM DarkZone dye and 10 mM 2,4-Dimethoxyaniline catalyst and were analyzed by FACS (32). E13.5 whole SMGs were manually dissected and cultured ex vivo for 24 h (41) and were incubated with DarkZone dye. Average fluorescence intensity was quantified using ImageJ (NIH). See *SI Appendix, Supplemental Methods* for details.

ALDH Enzymatic Assay. ALDH isozyme activity was measured spectrophotometrically (29) using 5 μg/mL of recombinant protein and 50 mM sodium pyrophosphate buffer (pH 7.4) in the presence of 2.5 mM NAD$^+$ and 10 mM substrate or with a fluorescence-coupled assay using 1 U/mL diaphorase and 0.1 mM resazurin (42). See *SI Appendix, Supplemental Methods* for details.

Docking of D-Limonene. D-limonene was prepared for docking using LigPrep (Schrödinger) and was docked to both ALDH2 and ALDH3A1 using their respective generated grids (the Alda-1 binding site for ALDH2 and the

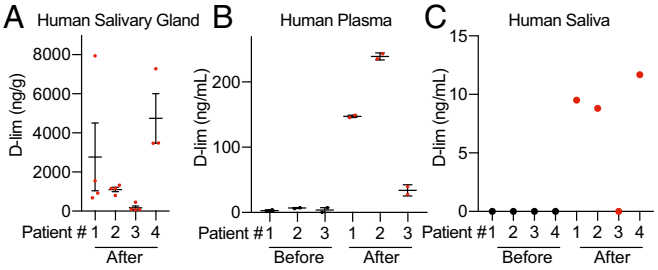

Fig. 5. Phase 0 human study of D-limonene drug distribution in four patients. (*A*) D-limonene levels in human salivary gland tissue collected after 2 wk of 2 g/d oral D-limonene measured by GC-MS ($n = 4$ tissue samples per patient; bars indicate SEM). (*B*) D-limonene levels in human plasma measured by GC-MS at baseline and after 2 wk of D-limonene treatment ($n = 2$ samples per patient per time point; the fourth patient was unable to provide plasma). (*C*) D-limonene levels in human saliva were measured by GC-MS at baseline and after 2 wk of D-limonene treatment ($n = 1$ sample per patient per time point).

analogous site for ALDH3A1). See *SI Appendix, Supplemental Methods* for details.

Stimulated Saliva Collection. Female C57BL/6J mice (9 to 11 wk old) were irradiated to the SMG. Pilocarpine (1.5 mg/kg) was delivered s.c., and saliva was collected for 15 min (14). See *SI Appendix, Supplemental Methods* for details.

PAS Staining and Acinar Quantification. Mouse SMGs were paraffin-embedded and stained with PAS (0.5%). Ten images per group were collected at random. The acinar area was quantified by RT Image software (43). See *SI Appendix, Supplemental Methods* for details.

RNA-Seq and Analysis. Sequencing data were generated on an Illumina HiSeq 4000 system. Genes that showed differential expression between groups were selected and analyzed using MetaCore (GeneGo). See *SI Appendix, Supplemental Methods* for details.

Annexin V/PI Apoptosis Assay. Dissociated $EpCAM^+$ salisphere cells were stained with annexin V and PI and were analyzed by FACS. See *SI Appendix, Supplemental Methods* for details.

Cleaved Caspase-3 Staining. Mouse SMGs were paraffin-embedded and stained with caspase-3 rabbit antibody (1:200; Cell Signaling) and DAPI. Three random images were taken from each gland and were quantified by counting cleaved caspase-3^+ cells per field. See *SI Appendix, Supplemental Methods* for details.

Phase 0 Study in HNC Patients. This study was approved by Stanford University Institutional Review Board, and written informed consent was obtained. D-limonene levels were measured with GC-MS with perillyl aldehyde as an internal standard (38). See *SI Appendix, Supplemental Methods*.

Statistical Summary. Data consisting of measurements collected at multiple time points were analyzed in a linear mixed-effects model to account for within-mouse correlation. Data that were measured at a single time point were analyzed in an ANOVA model. Post hoc testing of multiple pairwise comparisons was done using either a Tukey adjustment when comparing all possible pairs or a Dunnett's adjustment when comparing all groups with a single control group. A significance cutoff of 0.05 was used.

ACKNOWLEDGMENTS. We thank Sun Ten Pharmaceutical Co., Taiwan for the TCM library and the following researchers for their assistance: Dr. Yin-Ku Lin (TCM compounds), Dr. Vasilis Vasiliou (*Aldh3a1*$^{-/-}$ transgenic mice), Dr. Corey Liu (NMR), Dr. Ludmila Alexandrova (GC-MS), Dr. John Coller and Vida Shokoohi (RNA-seq), and Dr. Edward Graves (RT_Image software). All experiments were supported by NIH Grant R37 AA11147 (to D.M.-R.); NIH Grants R01 DE025227, P01CA067166, and U10CA180816 (to Q.T.L.); NIH Grant R01 GM110050 (to E.T.K.); and NIH Grants T32 GM089626 and T32 DK098132 (to L.D.V.W.).

1. Dirix P, Nuyts S, Van den Bogaert W (2006) Radiation-induced xerostomia in patients with head and neck cancer: A literature review. *Cancer* 107:2525–2534.
2. Kałużny J, Wierzbicka M, Nogala H, Milecki P, Kopeć T (2014) Radiotherapy induced xerostomia: Mechanisms, diagnostics, prevention and treatment–Evidence based up to 2013. *Otolaryngol Pol* 68:1–14.
3. Vergeer MR, et al. (2009) Intensity-modulated radiotherapy reduces radiation-induced morbidity and improves health-related quality of life: Results of a non-randomized prospective study using a standardized follow-up program. *Int J Radiat Oncol Biol Phys* 74:1–8.
4. Nutting CM, et al.; PARSPORT trial management group (2011) Parotid-sparing intensity modulated versus conventional radiotherapy in head and neck cancer (PARSPORT): A phase 3 multicentre randomised controlled trial. *Lancet Oncol* 12:127–136.
5. Vissink A, et al. (2010) Clinical management of salivary gland hypofunction and xerostomia in head-and-neck cancer patients: Successes and barriers. *Int J Radiat Oncol Biol Phys* 78:983–991.
6. Lovelace TL, Fox NF, Sood AJ, Nguyen SA, Day TA (2014) Management of radiotherapy-induced salivary hypofunction and consequent xerostomia in patients with oral or head and neck cancer: Meta-analysis and literature review. *Oral Surg Oral Med Oral Pathol Oral Radiol* 117:595–607.
7. Buglione M, et al. (2016) Oral toxicity management in head and neck cancer patients treated with chemotherapy and radiation: Xerostomia and trismus (Part 2). Literature review and consensus statement. *Crit Rev Oncol Hematol* 102:47–54.
8. Mercadante V, Al Hamad A, Lodi G, Porter S, Fedele S (2017) Interventions for the management of radiotherapy-induced xerostomia and hyposalivation: A systematic review and meta-analysis. *Oral Oncol* 66:64–74.
9. Hopcraft MS, Tan C (2010) Xerostomia: An update for clinicians. *Aust Dent J* 55: 238–244, quiz 353.
10. Pinna R, Campus G, Cumbo E, Mura I, Milia E (2015) Xerostomia induced by radiotherapy: An overview of the physiopathology, clinical evidence, and management of the oral damage. *Ther Clin Risk Manag* 11:171–188.
11. Grundmann O, Mitchell GC, Limesand KH (2009) Sensitivity of salivary glands to radiation: From animal models to therapies. *J Dent Res* 88:894–903.
12. Lombaert IM, et al. (2008) Keratinocyte growth factor prevents radiation damage to salivary glands by expansion of the stem/progenitor pool. *Stem Cells* 26:2595–2601.
13. Sugito T, Kagami H, Hata K, Nishiguchi H, Ueda M (2004) Transplantation of cultured salivary gland cells into an atrophic salivary gland. *Cell Transplant* 13:691–699.
14. Lombaert IM, et al. (2008) Rescue of salivary gland function after stem cell transplantation in irradiated glands. *PLoS One* 3:e2063.
15. Feng J, van der Zwaag M, Stokman MA, van Os R, Coppes RP (2009) Isolation and characterization of human salivary gland cells for stem cell transplantation to reduce radiation-induced hyposalivation. *Radiother Oncol* 92:466–471.
16. Nanduri LS, et al. (2011) Regeneration of irradiated salivary glands with stem cell marker expressing cells. *Radiother Oncol* 99:367–372.
17. Xiao N, et al. (2014) Neurotrophic factor GDNF promotes survival of salivary stem cells. *J Clin Invest* 124:3364–3377.
18. Pringle S, et al. (2016) Human salivary gland stem cells functionally restore radiation damaged salivary glands. *Stem Cells* 34:640–652.
19. Nanduri L, et al. (2013) Salisphere derived c-Kit+ cell transplantation restores tissue homeostasis in irradiated salivary gland. *Radiother Oncol* 108:458–463.
20. Banh A, et al. (2011) A novel aldehyde dehydrogenase-3 activator leads to adult salivary stem cell enrichment in vivo. *Clin Cancer Res* 17:7265–7272.
21. Coppes RP, Stokman MA (2011) Stem cells and the repair of radiation-induced salivary gland damage. *Oral Dis* 17:143–153.
22. Lombaert IM, Knox SM, Hoffman MP (2011) Salivary gland progenitor cell biology provides a rationale for therapeutic salivary gland regeneration. *Oral Dis* 17:445–449.
23. Pringle S, Van Os R, Coppes RP (2013) Concise review: Adult salivary gland stem cells and a potential therapy for xerostomia. *Stem Cells* 31:613–619.
24. Lombaert I, Movahednia MM, Adine C, Ferreira JN (2017) Concise review: Salivary gland regeneration: Therapeutic approaches from stem cells to tissue organoids. *Stem Cells* 35:97–105.
25. Chen CH, Ferreira JC, Gross ER, Mochly-Rosen D (2014) Targeting aldehyde dehydrogenase 2: New therapeutic opportunities. *Physiol Rev* 94:1–34.
26. Tateishi Y, Sasabe E, Ueta E, Yamamoto T (2008) Ionizing irradiation induces apoptotic damage of salivary gland acinar cells via NADPH oxidase 1-dependent superoxide generation. *Biochem Biophys Res Commun* 366:301–307.
27. Singh S, et al. (2013) Aldehyde dehydrogenases in cellular responses to oxidative/electrophilic stress. *Free Radic Biol Med* 56:89–101.
28. Ma I, Allan AL (2011) The role of human aldehyde dehydrogenase in normal and cancer stem cells. *Stem Cell Rev* 7:292–306.
29. Chen CH, Cruz LA, Mochly-Rosen D (2015) Pharmacological recruitment of aldehyde dehydrogenase 3A1 (ALDH3A1) to assist ALDH2 in acetaldehyde and ethanol metabolism in vivo. *Proc Natl Acad Sci USA* 112:3074–3079.
30. Xiao N, et al. (2013) A novel aldehyde dehydrogenase-3 activator (Alda-89) protects submandibular gland function from irradiation without accelerating tumor growth. *Clin Cancer Res* 19:4455–4464.
31. National Toxicology Program (2011) Safrole. *Rep Carcinog* 12:374–375.
32. Yuen LH, Saxena NS, Park HS, Weinberg K, Kool ET (2016) Dark hydrazone fluorescence labeling agents enable imaging of cellular aldehydic load. *ACS Chem Biol* 11: 2312–2319.
33. Maimets M, et al. (2016) Long-term in vitro expansion of salivary gland stem cells driven by Wnt signals. *Stem Cell Reports* 6:150–162.
34. Vigushin DM, et al.; Cancer Research Campaign Phase I/II Clinical Trials Committee (1998) Phase I and pharmacokinetic study of D-limonene in patients with advanced cancer. *Cancer Chemother Pharmacol* 42:111–117.
35. Sun J (2007) D-limonene: Safety and clinical applications. *Altern Med Rev* 12:259–264.
36. Perez-Miller S, et al. (2010) Alda-1 is an agonist and chemical chaperone for the common human aldehyde dehydrogenase 2 variant. *Nat Struct Mol Biol* 17:159–164.
37. Konings AW, Coppes RP, Vissink A (2005) On the mechanism of salivary gland radiosensitivity. *Int J Radiat Oncol Biol Phys* 62:1187–1194.
38. Miller JA, et al. (2013) Human breast tissue disposition and bioactivity of limonene in women with early-stage breast cancer. *Cancer Prev Res (Phila)* 6:577–584.
39. Nees DW, Wawrousek EF, Robison WG, Jr, Piatigorsky J (2002) Structurally normal corneas in aldehyde dehydrogenase 3a1-deficient mice. *Mol Cell Biol* 22:849–855.
40. Szlávik V, et al. (2008) Differentiation of primary human submandibular gland cells cultured on basement membrane extract. *Tissue Eng Part A* 14:1915–1926.
41. Steinberg Z, et al. (2005) FGFR2b signaling regulates ex vivo submandibular gland epithelial cell proliferation and branching morphogenesis. *Development* 132: 1223–1234.
42. Chen CH, et al. (2008) Activation of aldehyde dehydrogenase-2 reduces ischemic damage to the heart. *Science* 321:1493–1495.
43. Graves EE, Quon A, Loo BW, Jr (2007) RT_Image: An open-source tool for investigating PET in radiation oncology. *Technol Cancer Res Treat* 6:111–121.